Electro-optic dual-comb interferometer for high-speed vibrometry

(article starts on next page)

Electro-optic dual-comb interferometer for high-speed vibrometry

ELENA L. TELEANU,[1] VICENTE DURÁN,[1,2,3] AND VÍCTOR TORRES-COMPANY[1,*]

[1]*Department of Microtechnology and Nanoscience (MC2), Chalmers University of Technology, SE 41296, Gothenburg, Sweden*
[2]*Current affiliations: CNRS, LIPHY, F-38000 Grenoble, France and*
[3]*Université Grenoble Alpes, LIPHY, F-38000 Grenoble, France*
*torresv@chalmers.se

Abstract: Electro-optic frequency comb generators are particularly promising for dual-comb spectroscopy. They provide a high degree of mutual coherence between the combs without resorting to complex feedback stabilization mechanisms. In addition, electro-optic frequency combs can operate at very high repetition rates, thus providing very fast acquisition speeds. Here, we exploit these two features to resolve the rapid movement of a vibrating target. Our electro-optic dual-comb interferometer is capable of combining time-of-fight information with a more precise interferometric measurement based on the carrier phase. This fact, previously demonstrated by stabilized femtosecond frequency combs, allows us to increase the precision of the time-of-flight measurement by several orders of magnitude. As a proof of concept, we implement a fiber-based vibrometer that offers sub-nanometer precision at an effective acquisition speed of 250 kHz. These results expand the application landscape of electro-optic dual-comb spectroscopy to laser ranging and other remote sensing measurements.

References and links

1. I. Coddington, N. R. Newbury, and W. C. Swann, "Dual-comb spectroscopy," Optica **3**, 414-426 (2016).
2. I. Coddington, W. C. Swann, and N. R. Newbury, "Coherent multiheterodyne spectroscopy using stabilized optical frequency combs," Phys. Rev. Lett. **100**, 013902 (2008).
3. E. Baumann, F. R. Giorgetta, W. C. Swann, A.M. Zolot, I. Coddington, N. R. Newbury, "Spectroscopy of the methane v3 band with an accurate mid-infrared coherent dual-comb spectrometer," Phys. Rev. A **84**, 062513 (2011).
4. Zhaowei Zhang, Tom Gardiner, and Derryck T. Reid, "Mid-infrared dual-comb spectroscopy with an optical parametric oscillator," Opt. Lett. **38**, 3148-3150 (2013).
5. G. Villares, A. Hugi, S. Blaser, and J. Faist, "Dual-comb spectroscopy based on quantum-cascade-laser frequency combs," Nature Commun. **5**:5192 (2014).
6. I. Coddington, W. C. Swann, L. Nenadovic, and N. R. Newbury, "Rapid and precise absolute distance measurements at long range," Nature Photon. **3**, 351–356 (2009).
7. T.-A. Liu, N. R. Newbury, and I. Coddington, "Sub-micron absolute distance measurements in sub-millisecond times with dual free-running femtosecond Er fiber-lasers," Opt. Express **19**, 18501–18509 (2011).
8. S. Boudreau, S. Levasseur, C. Perilla, S. Roy, and J. Genest, "Chemical detection with hyperspectral lidar using dual frequency combs," Opt. Express **21**, 7411–7418 (2013).
9. S. Boudreau and J. Genest, "Range-resolved vibrometry using a frequency comb in the OSCAT configuration," Opt Express **22**, 8101–8113 (2014).
10. J. E. Posada-Roman, J. A. Garcia-Souto, D.A. Poiana, and P. Acedo, "Fast Interrogation of Fiber Bragg Gratings with Electro-Optical Dual Optical Frequency Combs," Sensors **16**, 2007 (2016).
11. F. Ferdous, D. E. Leaird, C.-B. Huang, and a M. Weiner, "Dual-comb electric-field cross-correlation technique for optical arbitrary waveform characterization," Opt. Lett. **34**, 3875–3877 (2009).
12. V. Durán, S. Tainta, and V. Torres-Company, "Ultrafast electrooptic dual-comb interferometry," Opt. Express **23**, 30557–30569 (2015).
13. T. Ideguchi, S. Holzner, B. Bernhardt, G. Guelachvili, N. Picqué, and T. W. Hänsch, "Coherent Raman spectro-imaging with laser frequency combs," Nature **502**, 355–358 (2013).
14. O. P. Lay, S. Dubovitsky, R. D. Peters, J. P. Burger, S.-W. Ahn, W. H. Steier, H. R. Fetterman, and Y. Chang, "MSTAR: a submicrometer absolute metrology system," Opt. Lett. **28**, 890-892 (2003).

15. G. Berkovic and E. Shafir, "Optical methods for distance and displacement measurements," Adv. Opt. Photon. **4**, 441-471 (2012).
16. J. Ye, "Absolute measurement of a long, arbitrary distance to less than an optical fringe," Opt. Lett. **29**, 1153-1155 (2004).
17. M. Cui, M. G. Zeitouny, N. Bhattacharya, S. A. van den Berg, H. P. Urbach, and J. J. M. Braat, "High-accuracy long-distance measurements in air with a frequency comb laser," Opt. Lett. **34**, 1982-1984 (2009).
18. J. Roy, J. -D. Deschênes, S. Potvin, and J. Genest, "Continuous real-time correction and averaging for frequency comb interferometry," Opt. Express **20**, 21932-21939 (2012).
19. T. Ideguchi, A. Poisson, G. Guelachvili, N. Picqué, and T. W. Hänsch, "Adaptive real-time dual-comb spectroscopy," Nature Commun. **5**:3375 (2014).
20. S.-J. Lee, B. Widiyatmoko, M. Kourogi, and M. Ohtsu, "Ultra-high scanning speed optical coherence tomography using optical frequency comb generators," Jpn. J. Appl. Phys. **40**, L878–L880 (2001).
21. A. J. Fleisher, D. A Long, Z. D. Reed, J. T. Hodges, and F. Plusquellic, "Coherent cavity-enhanced dual-comb spectroscopy," Opt. Express **24,** 10424–10434 (2016).
22. A. J. Metcalf, V. Torres-company, D. E. Leaird, and A. M. Weiner, "High-power broadly tunable electrooptic frequency comb generator," IEEE J. Sel. Top. In Quantum Electron. **19**, 350036 (2013).
23. K. Beha, D. C. Cole, P. Del'Haye, A. Coillet, S. A. Diddams, and S. B. Papp, "Electronic synthesis of light," Optica **4**, 406-411 (2017).
24. N. Kuse, T. R. Schibli, and M. E. Fermann, "Low noise electro-optic comb generation by fully stabilizing to a mode-locked fiber comb," Opt. Express **24**, 16884-16893 (2016).
25. X. Yi, K. Vahala, J. Li, S. Diddams, G. Ycas, P. Plavchan, S. Leifer, J. Sandhu, G. Vasisht, P. Chen, P. Gao, J. Gagne, E. Furlan, M. Bottom, E.C. Martin, M.P. Fitzgerald, G. Doppmann, and C. Beichman, "Demonstration of a near-IR line-referenced electro-optical laser frequency comb for precision radial velocity measurements in astronomy," Nat. Commun. **7**: 10436 (2016).
26. D. A. Long, A. J. Fleisher, K. O. Douglass, S. E. Maxwell, K. Bielska, J. T. Hodges, and D. F. Plusquellic, "Multiheterodyne spectroscopy with optical frequency combs generated from a continuous-wave laser," Opt. Lett. **39**, 2688–2690 (2014).
27. P. Martín-Mateos, B. Jerez, and P. Acedo, "Dual electro-optic optical frequency combs for multiheterodyne molecular dispersion spectroscopy," Opt. Express **23**, 21149 (2015).
28. G. Millot, S. Pitois, M. Yan, T. Hovannysyan, A. Bendahmane, T. W. Hänsch, and N. Picqué, "Frequency-agile dual-comb spectroscopy," Nature Photon. **10**, 27-30 (2016).
29. M. Yan, P. Luo, K. Iwakuni, G. Millot, T. W. Hänsch, and N. Picqué, "Mid-Infrared Frequency-Agile Dual-Comb Spectroscopy with Doppler-Limited Resolution," in *Conference on Lasers and Electro-Optics*, OSA Technical Digest (2016) (Optical Society of America, 2016), paper SW4H.4.
30. N. B. Hébert, V. Michaud-Belleau, C. Perella., G-W. Truog, J. D. Anstie, T. M. Stace, J. Genest, and A. N. Luiteu, "Real-Time Dynamic Atomic Spectroscopy Using Electro-Optic Frequency Combs," Phys. Rev. Appl. **6**, 044012 (2016).
31. V. Durán, P. A. Andrekson, and V. Torres-Company, "Electro-optic dual-comb interferometry over 40 nm bandwidth," Opt. Lett. **41**, 4190-4193 (2016).
32. N. B. Hébert, V. Michaud-Belleau, J. D. Anstie, J.-D. Deschênes, A. N. Luiten, and J. Genest, "Self-heterodyne interference spectroscopy using a comb generated by pseudo-random modulation," Opt. Express **23**, 27806 (2015).
33. R. Yang, F. Pollinger, K. Meiners-Hagen, J. Tan, and H. Bosse, "Heterodyne multi-wavelength absolute interferometry based on a cavity-enhanced electro-optic frequency comb pair," Opt. Lett. **39**, 5834-5837 (2014).
34. Multipoint Vibrometer, Optical Comb Inc. http://www.optocomb.com/
35. P. Castellini, M. Martarelli, and E. P. Tomasini, "Laser Doppler Vibrometry: Development of advanced solutions answering to technology's needs," Mech. Syst. Signal Process. **20** (6), 1265–1285 (2006).

1. Introduction

Coherent dual-comb spectroscopy (DCS) is an interferometric technique that exploits the resolution and accuracy offered by optical frequency combs to characterize spectroscopic samples in amplitude and phase [1]. The distinctive advantage of DCS is its ability of resolving individual comb lines whose spacing is usually finer than the resolution provided by standard commercial spectrometers [2]. This is possible thanks to the combination of two combs with slightly different repetition rates, enabling a virtual scanning over much longer delays than what is possible with conventional Fourier transform spectrometers. This feature is especially relevant in the mid- and far- IR region, where the strongest vibrational transitions in molecules are found [3-5].

DCS has made significant contributions in other metrology applications beyond the realm of spectroscopy, such as laser ranging [6-8], vibrometry [9,10], optical arbitrary waveform characterization [11,12] or coherent Raman spectral imaging [13]. For measuring distances,

DCS stands out due to its unique combination of high precision and large unambiguity range. Nanometer precision for an absolute range of > 1 m has been recently demonstrated [6], avoiding systematic errors due to spurious reflections that are observed in multiwavelength interferometric procedures [14]. This exceptional result is possible thanks to the combination of time-of-flight (TOF) information, a common method for laser ranging [15], together with an interferometric range measurement related to the phase of the optical carrier [16,17]. The use of free-running femtosecond fiber lasers can simplify dramatically the above dual-comb architecture, but at the expense of restricting the system to TOF measurements [7]. Alternatively, retrieving the full complex field with free-running combs requires the use of real-time signal processing techniques [18] or sophisticated adaptive schemes to compensate for relative drifts between the combs [19].

Electro-optic (EO) dual-comb interferometers constitute a DCS modality where the two combs are generated by external modulation of a continuous wave (CW) laser [20]. In these systems, the two comb generators are fed by the same laser, so optical phase locking between them is achieved by default, ensuring a high degree of mutual coherence [1]. This condition is essential to reach line-by-line spectral resolution, as well as to perform a long coherent averaging to increase the signal-to-noise ratio (SNR) [21]. EO frequency combs benefit from low-phase-noise microwave oscillators and high-performance lithium niobate modulators [22]. For absolute calibration of the wavelength axis, the CW laser can be locked to a radio-frequency standard via self-referencing [23], or with the aid of an additional self-referenced fiber laser frequency comb [24]. For less demanding applications in terms of absolute accuracy, the laser can be alternatively locked to a molecular absorption resonance [25]. EO dual-comb spectrometers have been reported for rapid and sensitive detection of molecular spectra across the near- [21, 26-28] and mid IR [29] regions. An important feature of EO combs is the possibility of operating at repetition rates exceeding 10 GHz, i.e. several orders of magnitude greater than the usual values offered by combs that rely on passive modelocking. This allows one to measure spectra at sub-microsecond rates [12], useful for resolving ultrafast dynamics in spectroscopy [30]. The bandwidth of the EO-dual-comb system can be expanded via coherent nonlinear broadening to a few THz [31] and the density of lines can be increased by external optical gating [32].

Cavity-enhanced EO combs with a relatively low frequency offset (~1 kHz) have been employed in multiwavelength interferometry for measuring distances up to 10 m [33]. However, the high refresh rates than can be attained with EO-DCS (>1 MHz) make it an ideal instrument for fast metrology applications, such as high-speed vibrometry. Indeed, scanless multipoint vibrometry has been already demonstrated by a commercial vibrometer that includes two EO frequency combs [34]. This commercial system is based on the principle of laser Doppler vibrometry, a widely used technique that time-resolves the Doppler-frequency shift produced by a moving target [15, 35]. The analysis of the frequency modulated signal generated through this effect leads to a measure of the time-dependent velocity of the target and its vibration amplitude. An EO-DCS can alternatively be combined with a fiber-based sensor to read distributed vibrations [10]. Notwithstanding, the optical phase coherence of the DCS is not fully exploited in these two examples. In this paper, we show high-speed vibrometry by measuring the interferometric term in combination with a time-of-flight measurement. In contrast with previous approaches that utilize EO frequency combs [33], we generate trains of subpicosecond pulses, which enables us to perform time gating for circumventing the systematic errors present in multiwavelength interferometry. In a proof-of-principle demonstration, we resolve sub-nanometer displacements from ultrasound vibrations operating at a maximum refresh rate of 250 kHz.

2.   Operation principle

2.1 Time-domain picture

Our experimental setup (depicted in Fig. 1) is basically the fiber-based interferometer described in detail in [12]. It includes two electro-optic frequency comb generators (signal and local oscillator, LO), fed by a CW laser, and a balanced detector (BD). Both combs have a frequency offset δf between them, $f_s = f_L + \delta f$, where $f_{s(L)}$ are the line spacings (repetition rates) of the signal and LO combs. This offset makes the system work as a 'virtual' scanning interferometer, since the pulses from each comb overlap on the detector at varying time delays. The relative time advance of the LO pulses in every signal period is $\delta t = T_L - T_S$, where $T_{s(L)} = f_{s(L)}^{-1}$. Therefore, to scan one period of the signal, $m = T_s/\delta t = f_L/\delta f$ periods of the LO are required, being m the so-called compression factor. The result of this repetitive process on the detector is an interference signal composed of a sequence of interferograms, each one containing a complete cross-correlation between the signal and LO electric fields. When one considers a dynamic sample that comprises a static reference element and a moving target (see lower inset in Fig. 1), two trains of pulses are generated in the signal arm and their relative time delay is encoded on the above cross-correlation.
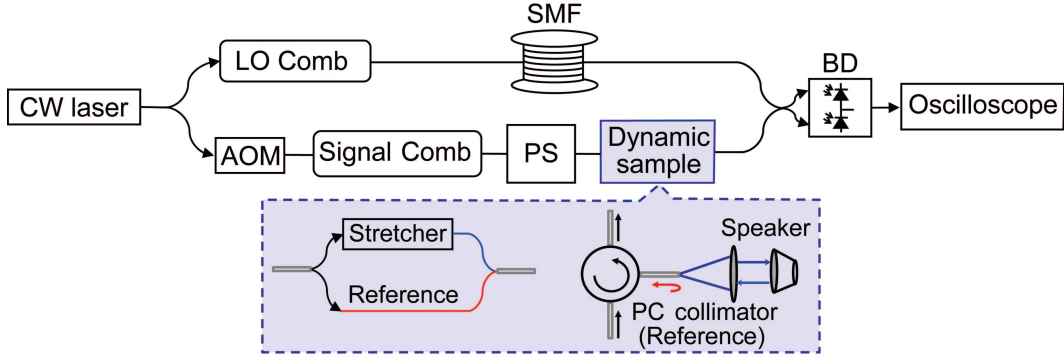

Fig. 1. Upper row: simplified electro-optic dual-comb spectrometer setup for vibrometry applications. Lower row: Examples of two dynamic samples used in this work (a fiber stretcher and an ultrasound speaker).

In our system, the comb generators operate at ~25 GHz and the offset between them is δf =100 MHz. The CW laser is centered at 1545 nm and has a linewidth of ~10 kHz. Both combs are composed of a pair of phase modulators followed by an intensity modulator. In the LO arm, a spool of single-mode fiber (SMF) is employed to impart onto the light spectrum a quadratic phase to achieve temporal pulse compression. In this way, LO pulses of around 800 fs are generated at the input of the detection system. In the signal arm, the light emerging from the comb is amplified by an erbium-doped fiber amplifier (EDFA, not shown in Fig. 1). A reconfigurable pulse shaper (PS), placed after the EDFA, is used to reduce the amplified spontaneous emission (ASE) noise due to the optical amplification and, in addition, to compress the signal pulses as in the LO arm. After passing through a dynamic sample, the signal pulses interfere with the LO, generating a photocurrent on the BD that is amplified in the electric domain and digitized with the aid of a real-time sampling oscilloscope (16 GHz bandwidth and sampling rate 50 GS/s).

2.2 Frequency-domain picture

In the frequency domain, the interference on the detector can be understood as a multi-heterodyne detection process, where each line of the signal beats with every LO line. The resulting beat notes are distributed along the radiofrequency (RF) region, leading to a downconversion of optical frequencies governed by the compression factor m. In an electro-optic dual-comb interferometer, this downconversion is, in principle, ambiguous, since both combs share the same central frequency. As a consequence, pairs of lines in the upper and lower

sidebands produce beat notes at exactly the same RF. In our experimental setup, an acousto-optic modulator (AOM) is inserted just before the signal comb (Fig. 1) to overcome this ambiguity [11]. The frequency shift introduced by the AOM is $f_{AOM} = 25$ MHz, a value that is of the same order as the frequency offset ($f_{AOM} \lesssim \delta f$) and commensurate to it ($f_{AOM} = \delta f/4$). The latter condition is ensured with an appropriate RF circuit for driving the AOM [12]. In the downconversion process, the induced frequency shift moves the interference between the central comb lines away from dc by f_{AOM} and creates two interleaved radio-frequency combs. With $f_{AOM} = \delta f/4$, the two interleaved combs simply lead to a set of equally spaced RF lines (located at $n\delta f/4$, being $n = 1, 3, 5, ...$). The net result is an RF comb with a line spacing $\delta f/2 = 50$ MHz and a global frequency offset of 25 MHz. This structure in the RF domain has the consequence that every interferogram is formed by four consecutive waveforms and its duration is $T = 1/f_{AOM} = 40$ ns, instead of 10 ns (the inverse of the frequency offset). Therefore, the maximum refresh rate of our system is 25 MHz. This value is reduced when coherent averaging is performed to increase the SNR of the acquired waveforms. The processing of the acquired temporal signal is analyzed in more detail in Section 3.

2.3. Dynamic samples

To exemplify the ability of our interferometer to deal with a dynamic sample, we have considered two different subsystems, both including a vibrating component (see lower inset in Fig. 1). The first one is an all-fiber setup where the signal arm is split in two paths by a 3-dB coupler, one of which contains a fiber stretcher as a vibrating element. Both paths differ in approximately 8 meters, so the differential dispersion between the pulses propagating through each path does not produce significant relative pulse broadening. The mentioned fiber stretcher consists of a piezo-electric cylinder with polarization-maintaining optical fiber rolled up around it. This piezo-electric component can introduce considerable delays (~ 1ps) between the two paths in response to a sinusoidal voltage. The working frequencies for the fiber stretcher can range from a few kHz to around 20 kHz.

The second subsystem includes in the signal arm a circulator and a free-space stage. The latter is formed by a collimator with a physical contact (PC) connector and a commercial piezo-speaker employed for generating ultrasounds (20-50 kHz). To increase the reflectivity, a thin metal plate is attached to the diaphragm of the speaker. The PC collimator is chosen deliberately to produce a strong reference reflection. This is very convenient in terms of robustness and stability, but it changes the reference to the fiber connector. This offset must be precisely calibrated for range-resolved measurements but it is not relevant when measuring the amplitude of high-speed vibrations. The light losses due to the free-space system and the relatively low target reflectivity make the internal reflection be ~20 dB stronger than the signal power coming from the target.

3. Data processing

3.1 Acquired temporal trace

Figure 2 shows an example of the recorded data during 160 ns (four consecutive interferograms). The sample for this example is the fiber stretcher. The oscilloscope uses as external clock the frequency offset δf between the combs, that is, a 100-MHz signal generated by an RF mixer from the signals driving the combs generators at 25 GHz and 25.1 GHz. The oscilloscope also registers the 25-MHz signal that feeds the AOM [12]. This auxiliary signal (upper curve in Fig. 2) allows us to extract individual interferograms.
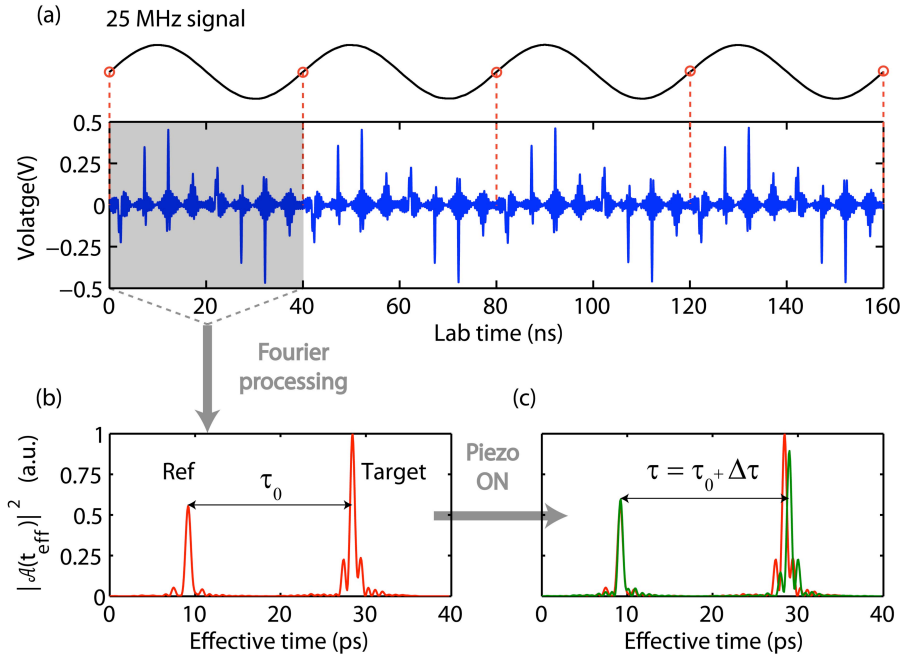
Fig. 2. a) Four consecutive interferograms recorded by the oscilloscope for the system that includes the fiber stretcher. The 25-MHz signal driving the AOM is registered simultaneously to extract every individual interferogram. b) Intensity of the temporal signal computed from a single interferogram. Two co-propagating pulses are reconstructed, one coming from the target and the other one from the reference, with a time delay τ_0 between them. c) When a voltage signal is applied to the fiber stretcher, the target pulse shifts by $\Delta\tau$ with respect to the reference peak. The two pulse profiles shown here (in red and green) correspond to two interferograms separated by 2 microseconds (5×10^4 optical periods).

The Fourier transform of every 40-ns interferogram provides the relative spectral complex amplitude of the signal comb. Indeed, for an ideal LO comb (with flat amplitude and constant phase), the retrieved RF comb is simply a down-converted version of the signal optical spectrum, where the spectral information of the sample has been encoded. For 100 consecutive interferograms (measurement time of 4 μs), the spectral signal-to-noise ratio (SNR_f) averaged over all the comb lines is $\overline{SNR_f} = 330$, which corresponds to an error in the spectral phase of 3 mrad. From the measured RF spectral components, the complex envelope $\mathcal{A}(t_{lab})$ of the signal field can be calculated, where t_{lab} (often called *laboratory time*) is defined on the time scale required to measure a single interferogram. More details about this calculation can be found in [12, 31]. In order to reconstruct the signal optical pulses, the downconversion nature of our measurements must be reversed, rescaling the complex pulse envelope $\mathcal{A}$ to t_{eff}, the so-called *effective time* scale (characterized by the time step $\delta t = T_L - T_S = 160\,fs$). A distinctive feature of our system is that 1000 optical periods of the LO are involved in every interferogram, instead of $f_L/\delta f = 250$. Therefore, the compression parameter is $m = 1000$, the ratio of the smallest comb repetition rate (25 GHz) to the frequency at which the interferograms are measured (25 MHz). This fact is due to the shift in the signal carrier frequency introduced by the AOM.

3.2 Processing of the temporal trace

The dynamic samples used in our system produce two co-propagating trains of pulses, one coming from the vibrating element (target) and the other from the reference [Fig. 2(b)]. The relative time delay τ_0 between them changes in accordance to the vibration of the sample. In this work we focus on the precision of the EO-DCS system, not on its absolute accuracy. For

this reason, we restrict ourselves to measuring the variation $\Delta\tau$ of the relative time delay along the complete sequence of interferograms [Fig. 2(c)]. In our measurements, $\Delta\tau$ is always much lower than the initial time shift τ_0 between the pulses. The amplitude of the target vibration is calculated from $\Delta\tau$ using the light group velocity v_g in the considered propagation medium.

Here, we perform the vibration analysis in the frequency domain, using the Fourier transform $\mathcal{V}$ of the pulse complex envelope $\mathcal{A}$. To find the relative delay between the target and the reference pulses, their contributions to the signal are time-gated using Blackman windows, which are carefully centered around every pulse peak [6, 28]. This process creates two copies of every recovered signal, each one containing only a single pulse. Then, the spectral envelope functions for the reference and the target contributions, $\mathcal{V}^r$ and $\mathcal{V}^t$, differ in a linear phase factor, $\exp[i\,\phi(\nu)]$, where $\phi(\nu) = \phi_0 + b(\nu - \nu_0)$, where ν_0 the optical carrier frequency [6]. The slope m of this relative phase is related to the TOF measurement through $\tau = b/2\pi$, as can be directly derived from the time-shift property of Fourier transforms. The corresponding distance, assuming a round trip of light, is $L_{TOF} = \tau\,v_g/2$ and its ambiguity range is given by $R = T_S\,v_g/2$. For our vibrometer, the ambiguity range is 6 mm. Thanks to the fact that we use a single CW laser to generate both combs, ϕ_0 (the relative phase at the carrier frequency) provides an independent distance measurement, $c\,\phi_0\,/(4\pi\nu_0 n)$, where c is the speed of light and n is the phase refraction index calculated at ν_0. Since the ambiguity range of this interferometric measurement is limited to half the carrier wavelength (for our system, ~0.8 μm), any distance beyond that range is given by $L_{int} = c\,(\phi_0 + 2\pi m)\,/(4\pi\nu_0 n)$, where m is an integer. This ambiguity can be solved using additional information about the target distance (for instance, the TOF information). From the expression for L_{int}, it is apparent that the precision of the interferometric measurement depends not only on the error in the spectral phase ϕ_0 (given by the SNR per spectral bin), but also on the carrier frequency precision. For our system, the laser drift is negligible during the signal acquisition time, so the precision of L_{int} is hence limited by the spectral phase error. However, the accuracy of the interferometric measurement depends on the absolute knowledge of the carrier frequency. For very demanding applications, where systematic distance errors must be minimized, the accuracy can be increased by stabilizing the CW laser to a molecular reference or a self-referenced frequency comb.

Coherent averaging of measurements leads to an increase of their SNR at the expense of reducing the refresh rate [1]. Given the dynamic nature of our measurements, the above averaging process has to be performed in such a way that it does not hinder the time evolution of the sample. Here, we employ a moving average that involves a subset N_{avg} of consecutive measurements obtained at the maximum speed, f_{AOM}. As a consequence, the effective refresh rate becomes $f_{er} = f_{AOM}/N_{avg}$. The key point of this averaging process is the choice of N_{avg} to avoid artifacts when a dynamic vibration is resolved. In our experiments, the frequency at which the sample vibrates is $f_s \leq 50$ kHz, so fixing $N_{avg} = 100$ ensures that $f_{er} \geq 5f_s$.

4. Experimental results

4.1. Electro-optic dual-comb vibrometry

Figure 3 summarizes the results for the vibration of the fiber stretcher when it is driven by a sinusoidal voltage at 20 kHz. We analyze a 160-μs oscilloscope trace (4000 consecutive interferograms). As can be observed in Fig. 3(a), the TOF measurement clearly shows a sinusoidal evolution of $\Delta\tau$. The blue dots correspond to the values of $\Delta\tau$ retrieved when the interferometer operates at the maximum refresh rate. Every point is hence the result of processing an individual interferogram. To reduce the data error, we use a moving average that involves an optimal subset of N_{avg} points. Once N_{avg} is fixed, we calculate the mean value that is the result of averaging the data from the first value of $\Delta\tau$ to the N_{avg}-th one. This averaged delay is assigned to the time point $N_{avg}T/2$, being T the acquisition time of a single

interferogram. Then, we average a data subset from the second point to the $(N_{avg} + 1)$-th one, assigning this second mean delay to the instant $N_{avg}T/2 + T$, and so on. Following this procedure with $N_{avg} = 100$ ($f_{er} = 250$ kHz) the red curve shown in Fig. 3(a) is built up, demonstrating an apparent reduction of the data dispersion. Figure 3(b) shows the time evolution of the unwrapped carrier phase at 250 kHz. The consistency of this result and the one obtained by TOF can be checked easily. For example, the peak-to-peak value of the unwrapped ϕ_0 can be expressed as a distance using the central laser frequency ν_0 and the corresponding phase refraction index for a standard single-mode fiber. Alternatively, that distance can be calculated from the delay measured by the TOF, taking into account the group velocity inside the fiber. Both values result to be clearly compatible, differing in around 450 nm (0.25% of the measured distance).
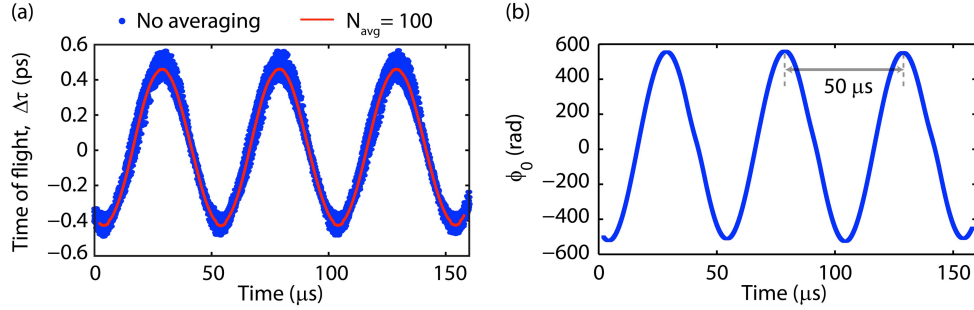

Fig. 3. Time-resolved vibration of the fiber stretcher driven by a sinusoidal signal at 20 kHz. (a) TOF measurements at the maximum refresh rate (25 MHz) and when a moving average is performed (effective refresh rate of 250 kHz). The reduction of the data noise in the second case is apparent. (b) Temporal evolution of the unwrapped spectral phase of the carrier, showing the expected behavior with a period of 50 μs.

The experimental results for the ultrasound speaker working at 50 kHz can be observed in Fig. 4. We process an 80-μs trace, that is, 2000 consecutive interferograms. Despite the voltage signal applied to the speaker has the maximum attainable amplitude, the delay $\Delta\tau$ cannot be resolved using TOF information, even with 100x coherent averaging. This lack of precision of the TOF results is explained in detail in the next subsection. On the contrary, the recovered ϕ_0 after applying an unwrapping algorithm shows the expected sinusoidal behavior. This oscillation expressed in terms of distances reveals a movement with a sub-micrometer amplitude. A direct calculation from ϕ_0 gives a value of 630 nm for the vibration amplitude, assuming a negligible Gouy phase shift for the displacement range considered here. This corresponds to a maximum $\Delta\tau$ of 4 fs, which cannot be resolved with the precision of the TOF (see next subsection).

Fig. 4. Time-resolved vibration of the piezo-speaker driven by a sinusoidal voltage signal at 50 kHz. (a) TOF measurements showing the inability of this procedure to resolve the speaker movement. (b) Temporal evolution of the unwrapped spectral phase of the carrier, where the vibration can be resolved without problem.

4.2. Precision analysis

To test the performance limitations of our laser ranging system, we conduct measurements when no voltage is applied on the vibrating element, so the delay τ_0 remains constant over time. The precision attained by TOF is then evaluated as the standard deviation of $\Delta\tau$, $\sigma_{\Delta\tau}$, and the interferometric precision is given by the standard deviation of ϕ_0, σ_ϕ. Following the averaging process described in the preceding section, we calculate both statistical parameters as a function of the averaging window t_{avg}, defined as $t_{avg} = N_{avg}\,T$. The result can be observed in Fig. 5. The precision of the TOF method is ultimately limited by the jitter in the relative timing of the retrieved signal pulses, whereas the phase jitter of the CW laser determines the limit in the attainable precision of the interferometric phase term ϕ_0. In both cases, the well-known tradeoff between measurement speed and precision is evidenced by the evolution of the standard deviations. For our system, the interferometric measurement is always >500 times more precise than the result by TOF. We can illustrate this fact with the results obtained for the speaker vibration when $t_{avg} = 4\,\mu s$ (that is, at the equivalent measurement rate of 250 kHz considered in previous figures). The standard deviation of $\Delta\tau$ ($\sigma_{\Delta\tau} = 3.6\,fs$) leads to a distance precision of 500 nm. This value is very similar to the one previously derived for the total amplitude of the speaker displacement. As a consequence, the TOF procedure fails to resolve the speaker movement. On the contrary, the phase jitter amounts to 6.5 mrad for the same averaging window, which is equivalent to a precision of 0.8 nm.
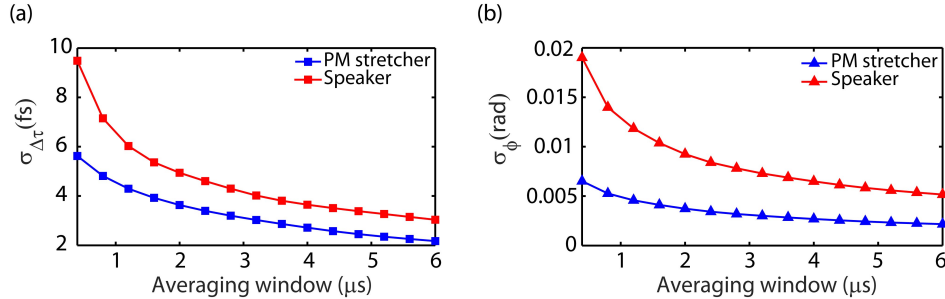

Fig. 5. Analysis of precision measurement in our EO dual-comb vibrometer. (a) Relative timing jitter between the reference and the target pulses for different averaging windows. (b) Phase jitter of the interferometric measurement for different averaging windows.

5. Conclusions

In this paper, we have employed an EO dual-comb interferometer for measuring time-varying waveforms generated by two vibrating targets (at frequencies up to 50 kHz). The variable delay between the co-propagating trains of pulses generated by these dynamic samples has been measured using two different procedures. With a TOF measurement, delays of around 1 ps (i.e., equivalent to distances of ~0.1 mm) have been measured with a precision of a few femtoseconds at an equivalent measurement rate of 250 kHz. Since the ambiguity range R scales as $1/f_s$, it can be easily tuned. Using any laser ranging technique with a precision lower than R, it is possible to choose the stand-off distance at which the vibrometry measurements are performed, although this distance is ultimately limited by the system sensitivity. As it was demonstrated in [12], our dual-comb system can work in low-light-level scenarios by means of a pre-amplified detection scheme. Apart from the TOF method, we have demonstrated a second measurement based on recovering the complex amplitude envelope of the optical signal coming

from the target. This is a distinctive feature of coherent DCS that cannot be achieved by laser Doppler-based measurements. From this measurement, it is possible to reach sub-nanometer precision. This value implies a relative precision level of 1.3×10^{-7} for 6 mm of measurement range. The above results expand the use of EO-DCS systems and indicate that the phase coherence inherently available in this spectroscopy modality can be effectively utilized in high-precision ultrafast metrology applications.

Funding